Contributions to Geophysics and Geodesy Vol. 48/2, 2018 (133–160)

An optimal multiscale approach to interpret gravity data using successive decomposition of the Bouguer anomaly

Mohamed ARFAOUI[1,2], Mohamed Hedi INOUBLI[2], Adnen AMIRI[2]

[1] Office National des Mines,
24, Rue de l'Energie, 2035, La Charguia, Tunis, Tunisia; e-mail: mohamarfaoui@gmail.com

[2] Unité de Recherche de Géophysique Appliquée aux Matériaux et aux Minerais, Université Tunis-El Manar, Faculté des Sciences de Tunis, 2092 El Manar, Tunis, Tunisia

Abstract: A multiscale interpretive approach is presented to identify multiscale discontinuities and sources boundaries, and to obtain comprehensive pseudo-section density images of 2D structures at depth. This interpretive approach is based on the total horizontal gradient and apparent density operator applied to the gravity anomalies of pseudo-depth slices derived from the successive decomposition of the Bouguer anomaly. This approach is applied to gravity data from the northwestern part of Tunisia, it provides the fault system repartition at different depths and describes the density distribution within the basins and trough. Thus, the NW–SE and NE–SW faults are the deepest whereas the N–S and E–W faults are relatively superficial. The density pseudo-sections reveal the vertical continuity of salt Triassic outcrops of Jebel Debadib as well as a diapiric model, the presence of a Triassic salt dome in the Kalaa El Khasba through and dense series under the Miopliocene and Quaternary deposits of the Mejarda basin.

Key words: Gravity anomalies, Tunisia, Multiscale discontinuities, Pseudo-depth slices, Pseudo-section density

1. Introduction

Gravity surveys are designed to delineate geologic structures at depth by interpretation of observed data. The essential question is to find a quantitative and qualitative interpretive process for determining 3D locality and density of causative sources. Generally interpretation of gravity data follows three principle strategies: (1) anomaly separation, (2) identifying source boundaries and discontinuities, and (3) resolving sources at depth, which includes depth determination and source density.

doi: 10.2478/congeo-2018-0005

Anomaly separation into regional and residual components by decomposition is commonly used in gravity interpretation. Short wavelength components associated with near surface geologic bodies are separated from long wavelength features associated with deep seated structures. Decomposition may be achieved by least squares fitting of polynomial surfaces (*Simpson, 1954*), wavenumber filters as an upward continuation (*Gupta and Ramani, 1980*), Gaussian function (*Arfaoui et al., 2015*), or bandpass Wiener optimum filters (*Pawlowsky and Hansen, 1990*). Since the Bouguer anomaly is the sum of several components caused by deep seated, intermediate and near surface geologic bodies the gravity effect of those sources may be estimated from a successive decomposition process where the decomposition "bootstraps" to greater depths with each iteration (*Arfaoui et al., 2011*).

Sources boundaries and discontinuities are usually defined by several different derivative operators. These discontinuities generally correspond with high density contrast zones associated with geological contacts and faults. Various derivative operators have been developed for enhancing the gravity signal. They are designed using a combination of simple gravity gradients and have been tested by many studies. One fundamental study was realized by *Cordell and Grauch (1982, 1985).* They used the maximum total horizontal gradient to map boundaries between domains of uniform density and magnetic susceptibility. The use of this operator was improved and automated (*Blakely and Simpson, 1986*) by assigning a quality factor to the maximum gradient after comparing each point of the grid with its neighbors. *Miller and Singh (1994)* and *Verduzco et al. (2004)* introduced the tilt angle (TDR) and the total horizontal derivative of the tilt angle (THDR), respectively, which are relatively powerful operators to detect boundaries between areas having a density contrast. The high resolution standardized operators such as the Theta map, horizontal tilt angle (TDX) and E-Tilt, are elucidated by *Wijns et al. (2005)*, *Cooper and Cowan (2006)* and *Muzaffer and Ünal (2013)*, respectively. Despite the high resolution of the derivative operators, the discontinuities and source boundaries derived from their application to the Bouguer anomaly, represent a resultant of different source components seated at different depths. *Fedi and Florio (2001)* presented a multiscale derivative analysis (MDA) based on the enhanced horizontal derivative (EHD). This multiscale analysis allows the determination of source boundaries and discontinuities at different depths.

The first two principal strategies concern themselves with resolving the discontinuities and boundaries of geologic sources while the third is concerned with source characterization. Numerous quantitative interpretations of potential field anomalies are developed after calculation of simple source effects by *Nettleton (1942)*. Despite the complexity of the resolution process caused by the nonlinearity, methods were developed to assess the source parameters from the potential field anomalies as the Werner deconvolution (*Werner, 1953*) and the Euler deconvolution (*Thompson, 1982*).

The latest application was developed by *Reid et al. (1990)* for the interpretation of 2D data. Other applications of Euler deconvolution applied to the analytic signal and the enhanced analytical signal are introduced by *Keating and Pilkington (2004)* and *Salem and Ravat (2003)*, respectively. The source parameters imaging method (SPI) developed by *Thurston and Smith (1997)* is also effective for the evaluation of source parameters of potential field anomalies. The 2D forward modeling of density contrasts at depth has occupied equally an important place in quantitative gravity interpretation studies. The 2D modeling generates geometrical shape and physical properties which provide the closest calculated anomaly to the observed one (*Talwani et al., 1959; Talwani and Ewing, 1960*). However, density contrasts with depth are generally determined using inversion techniques (*Last and Kubik, 1983; Mareschal, 1985; Murthy and Rao, 1993*).

In this paper, we present a multiscale interpretive approach adopted for the three gravity modeling techniques based on the successive decomposition of the Bouguer anomaly. This approach first determines discontinuities and boundaries of sources at different depths in the first step. In the second step, the imaging of density repartition at depth is resolved. This approach was applied to gravity data from northwestern Tunisia with satisfactory results.

2. Processing and methodology

Potential field anomalies are dissociated into residual and regional anomalies using a method of separation. Several pairs of regional and residual anomalies can be obtained from each separation method by changing the director parameter. However, it is possible to separate the Bouguer anomaly into

several components, since it is the sum of the gravity effects of superimposed geological structures situated at different depths. Therefore, several multi-component decomposition scenarios of Bouguer anomaly are possible as the successive decomposition developed by *Arfaoui et al. (2011)*.

Successive decomposition was used to decompose the gravity anomaly with a pseudo-depth slicing scheme (Fig. 1). It was carried out in first step to dissociate the Bouguer anomaly into several pairs of residual and regional anomalies associated with different controlling parameters, which correspond to different pseudo-depths of separation. The second step concerns the dissociation of the residual anomaly corresponding to the pseudo-depth P_i to two anomalies by subtracting the residual anomaly on the pseudo-depth P_{i-1} ($P_{i-1} < P_i$), and we obtained:

– The gravity anomaly of the pseudo-depth slice sited between the pseudo-depths P_i and P_{i-1}.
– Residual anomaly on the P_{i-1} depth.

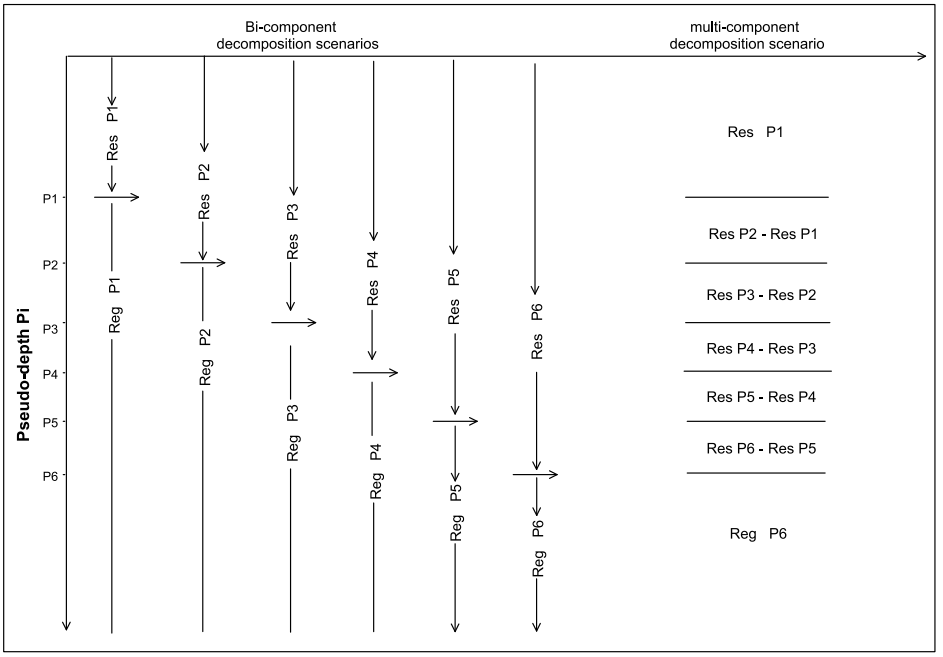

Fig. 1. Successive decomposition of the Bouguer anomaly.

The next steps consist to determining the gravity effects of the pseudo-slice located between the pseudo-depths P_{i-1} and P_{i-2} by the deduction of the residual anomaly corresponding to the pseudo-depth P_{i-2} from the residual anomaly associated to the pseudo-depth P_{i-1}. Thus, the successive decomposition of the Bouguer anomaly using a given separation method, leads to gravity anomalies of several pseudo-depth slices located between the pseudo-depths P_i and P_{i-1}, whose sum is equal to the Bouguer anomaly (Fig. 1).

We decompose the gravity anomaly with a pseudo-depth slicing scheme using the Gaussian filter as a separation method (Fig. 1). Spectral depth analysis in the wavenumber domain (*Spector and Grant, 1970; Negi et al., 1986; Maus and Dimri, 1996; Bansal and Dimri, 2001*) is then used for approximating pseudo-depths of pseudo-slice interfaces. We applied the spectral depth analysis method to estimate depths of the causative sources of anomalies in residual maps associated with standard deviation of Gaussian filter equal 0.4, 0.3, 0.2, 0.1, 0.05 and 0.02 cycle km^{-1}, which approximate the pseudo-depths of pseudo-slice interfaces. The logarithm of the radial average of the energy spectrum of each residual map was plotted versus the radial frequency (Fig. 5). The half slope of each linear segment of the spectrum corresponds to the mean depth of the causative sources of anomalies in the residual maps.

The total horizontal gradient operator is applied to the gravity of pseudo-depth slices derived from the successive decomposition of the Bouguer anomaly to produce horizontal gradient maps at different pseudo-depths. The maxima of this operator correspond to the abrupt density variation zones associated to geological contacts and faults.

The apparent density operator is applied equally to the gravity of pseudo-depth slices to establish apparent density maps at different pseudo-depths from which we evaluate pseudo-density sections. The apparent density operator is performed in the wavenumber domain which assumes that a horizontal layer of fixed thickness and density variable could explain the gravity signal. The operator determines the contrast of the apparent density in the wavenumber domain as expressed in the equation (1) given by *Gupta and Grant (1985)*:

$$L(r) = \frac{r}{2\pi G}\,(1 + e^{-tr})^{-1}\,, \tag{1}$$

where G is the gravitational constant, r is the wavenumber and t is the thickness of the equivalent layer (pseudo-slice). The apparent density maps were calculated by using a thickness equivalent layer equal to the thickness of the pseudo-depth slices. Thus, the thickness of 490, 150, 350, 400, 1210 and 1950 m are used for the gravity anomaly of pseudo-slices 1, 2, 3, 4, 5 and 6 (Fig. 6), respectively. Taking into consideration density values of 350 surface samples and the repartition of outcrops, the background densities of 2.25, 2.28, 2.3, 2.33, 2.38 and 2.42 g/cm^3 are adopted for the calculus of apparent density maps of the pseudo-slices 1 to 6.

The six apparent density maps associated the maps of different slices were used to established density pseudo-slice sections. The apparent density data of each profile are then extracted from the six apparent density maps profiles, combined and attached to pseudo-depths of the anomaly separation interface. After, they are gridded by profile to generate apparent density pseudo-section.

3. Application of the interpretive approach to field case

3.1. Geographic and Geological settings of the study area

The study area is located in the northwestern part of the Tunisian Atlas. It extends from Kalaa El Kasba in the South to Jebel Hairech in the North (Fig. 2).

The study area is located at the front of the nappe zone. It is characterized by folding tectonic, Atlasic type deformation and salt structures. It includes the western parts of three different geological domains: the Mejarda basin in the North, the diapir zone in the middle and the central Tunisian Atlas in the South. Furthermore, the northern part of the study area includes the Permo-Triassic, Triassic, Jurassic and Cretaceous structures, which generally constitute the Mejarda basin limits (Fig. 3). The diapiric zone includes Triassic and Aptian anticlines, Early Eocene synclines and Mio-Pliocene and Quaternary filled depressions. The most notable feature of the southern section is the Kalaa El Khasba through filled with Mio-Plio-Quaternary deposits (*Chihi, 1995*) and the Aptian Recifal limestone outcrops in the form of resistant structures that dominate the relief (*Mahjoubi, 1978; Smati, 1986*). Northwest-southeast and northeast-

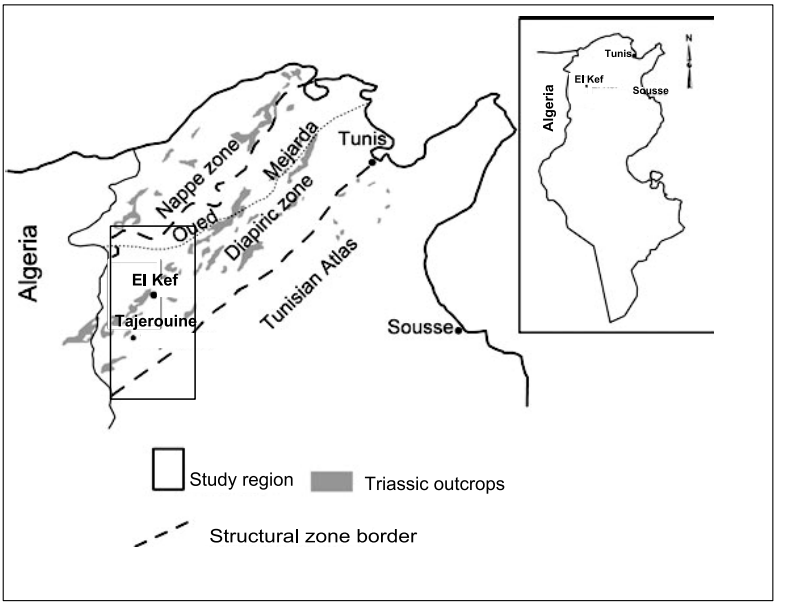

Fig. 2. Location of the study region.

southwest trending faults locally marked by Triassic material, exert control on these structures that are also cut by north-south and east-west trending transverse faults (*Sainfeld, 1951; Burollet and Sainfeld, 1956b; Chikhaoui, 2002; Smati, 1986; Burollet, 1991; Zaier, 1999b; Ould Begga, 2003; Amiri, 2013*). The post-Albian series varies laterally in thickness and facies in response to geodynamic and depositional processes (*Perthuisot, 1978*). Thus, the reduced carbonate series and gaps in the sedimentary sequences may be identified close to Triassic outcrops (Fig. 3). These sequences confirm up-shoaling strata at the emplacement of actual Triassic extrusions (*Perthuisot, 1978; Perthuisot et al., 1998*). Thick and complete sedimentary series with a major marl component are deposited in rim-synclines (Mellègue's dam, Oued Bou Adila area, Jebel Bou Lahnèche and Jebel Jerissa). Since Late Aptian time, the structural evolution of this region has been controlled by successive extensional and compressive tectonic events related to halokinesis (*Perthuisot, 1978; Perthuisot et al., 1998; Chikhaoui, 2002*). The structures comprising basins and Cretaceous up-shoaling were strongly influenced by Tertiary tectonics, thus initiating anticlines, synclines and collapsed troughs.

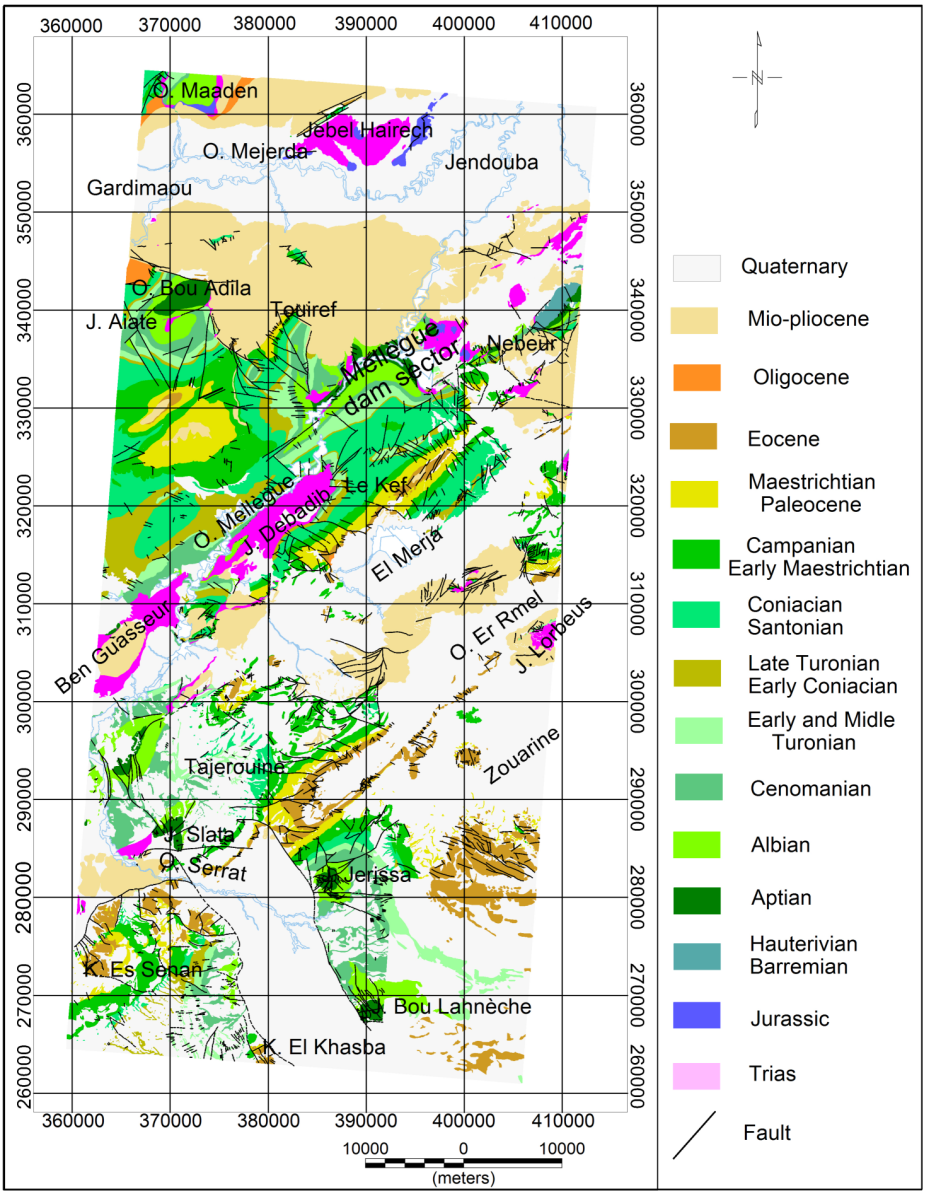

Fig. 3. Geological map of the study region adapted from *Sainfeld (1951), Gottis and Sainfeld (1955), Burollet and Sainfeld (1956a and 1956b), Lehotsky (1979), Lehotsky and Bujnowsky 1995, Ben Haj Ali (1997), Mahjoub (1997), Fakhraoui et al. (1998), Zaier (1999a).*

The main structures (Fig. 3) of the study area are:

- The Mejarda Basin filled by Mio-Pliocene-Quaternary deposits,
- The salt Triassic structures explained by the diapir and salt glacier models (*Ghanmi et al., 2000; Perthuisot et al., 1998; Rouvier et al., 1998; Vila et al., 1994; 1996*),
- The Kef trough sited in the SW Tunisian furrow boundary, is filled by Mio-Pliocene-Quaternary sediments,
- The Kalaa El Khasba trough is a part of the offset graben system of Rohia, Kalaa El Khasba and Ouled Bou Ghanem. It is filled with Mio-Pliocene-Quaternary deposits.

3.2. Gravity anomaly

The Bouguer anomaly represents all mass heterogeneities in depth. Usually the most interesting result from gravity surveys occurs when the survey reveals lineaments that are not observed at the surface. The Bouguer anomaly map also provides important information on the nature of geological structures, and structural directions. A total of 4852 gravity stations from five surveys acquired at 1 km intervals are used in this paper. These gravity surveys belong to a current Tunisia gravity project conducted by the Office National des Mines (Tunisia). It was begun in 1996 as systematic and long term gravity coverage with a 1 station per km^2 for all of Tunisia. Consistent high quality standards in gravity data and elevation control have been maintained since the start of the project. The gravity data acquisition and processing and accuracy standards are described in more detail in previous papers (*Arfaoui et al., 2011; Arfaoui and Inoubli, 2013*).

The Bouguer anomaly map of the study area shows southern and northern domains occupied by long-wavelength negative and positive anomalies, respectively. They are separated by an intermediary domain characterized by short and medium wavelength anomalies (Fig. 4). The northern domain includes the Medjerda Basin and Permo-Triassic, Jurassic and Cretaceous structures of Jebel Hairech and Oued Maaden. It is dominated by long wavelength positive anomalies oriented following E–W and NE–SW directions; with amplitudes ranging between –20 and 13 mGal. Moreover, this domain indicates near surface high density bodies under the Pliocene-Quaternary

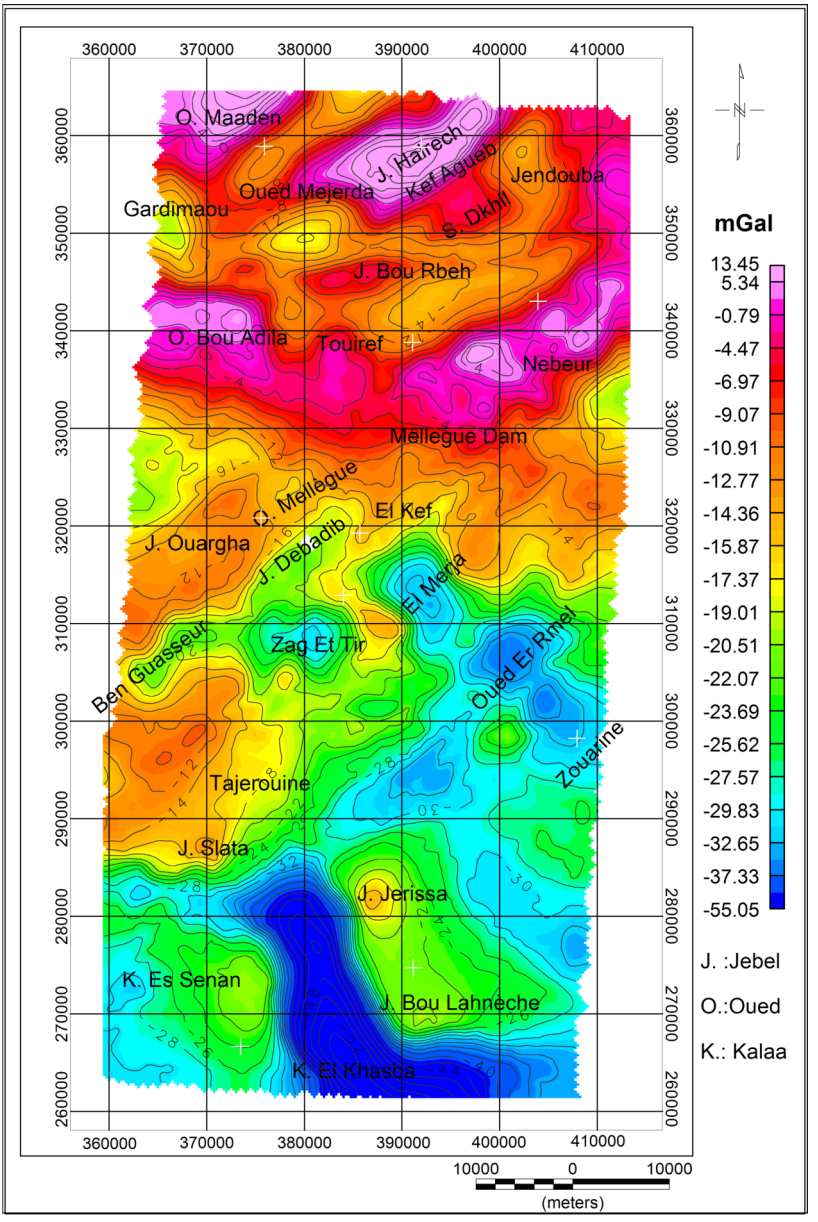

Fig. 4. Bouguer anomaly map.

cover (Fig. 4). The middle domain comprises the Ouargha- El Kef region and its surroundings. It is characterized by short and medium wavelength NE–SW and NW–SE anomalies. It is characterized by positive anomalies coinciding with Quaternary deposits in El Kef and Zouarine plains. They correspond to Cretaceous and/or Eocene structures. The southern domain extends to the south of Tajerouine and is essentially defined by negative

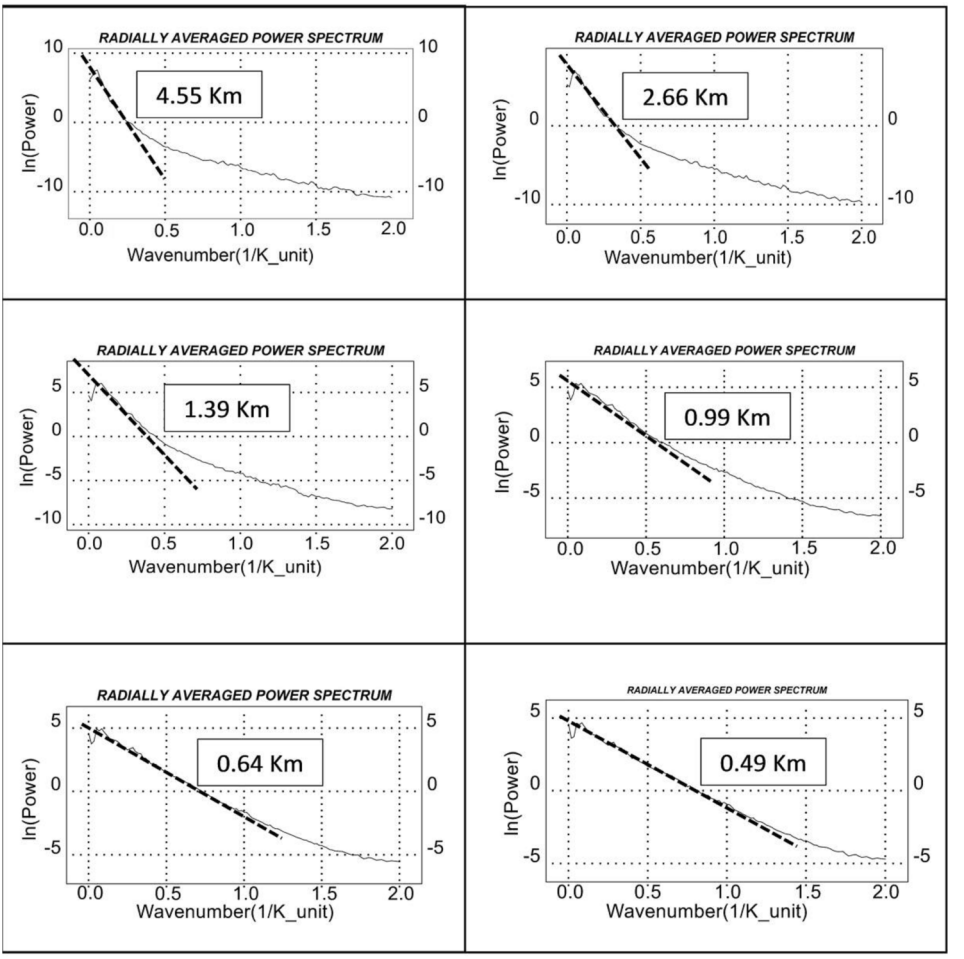

Fig. 5. Radially averaged spectrum of residual maps. Sp Res Gaussian filter 0.3: radially averaged spectrum of the residual map obtained by Residual/ Regional Gaussian filter with standard deviation equal 0.3 cycle km^{-1}.

NW–SE anomalies with amplitudes reaching –55 mGal. The most important one is the Kalaa El Khasba Trough (Fig. 4).

The NW–SE and NE–SW trending gravity lineaments observed on the Bouguer anomaly map correspond to outcropping structures (Kalaa Khasba and El Kef troughs, salt Triassic structures of Jebel Debadib- Ben Gasseur...). They present interruptions and spatial shifts and high gradients along certain anomalies which reflect faults and their effects. The Mio-Plio-Quaternary deposits are associated with two types of anomalies: negative anomalies corresponding to low density material filling collapsed zones and positive anomalies comparable to those observed in the Triassic and Cretaceous series. The positive anomalies are not related to Quaternary deposits but rather support the presence of mass excess. These are attributed to the Triassic and/or Cretaceous and Eocene dense rocks bordering the previously defined collapsed zones. Thus, the positive anomalies situated to the southeast of Jebel Hairech and in the plains of Jendouba and El Kef which coincide with quaternary units are actually caused by denser rocks under the quaternary cover.

In the north, the Jebel Hairech Permo-Triassic and Kef Agueb Jurassic structures belong to a NE–SW positive gravity anomaly which extends to the NE and SW crossing Quaternary units. This confirms the continuity of these structures under the Quaternary overburden. Moreover, the Jebel Hairech structure is bordered by relatively high gradient zones indicating the presence of significant faulting. They appear to have played an important role in the evolution of this structure (Fig. 4). The anomaly amplitudes associated with geological series of same age increase from south to north.

Generally the Bouguer anomaly map explains the majority of mapped outcrops, but it also reveals uncorrelated anomalies, that are probably caused by deeper structures. Resolving the Bouguer anomaly into residual and regional components can resolve the near surface and deeper sources.

3.3. Successive decomposition of the Bouguer anomaly

Successive decomposition of the Bouguer anomaly into several components, using the Gaussian filter as a separation method, allows the review of mainly structural features and the analysis of density variation in depth (Fig. 6). The regional anomaly derived from the Gaussian filter of standard deviation

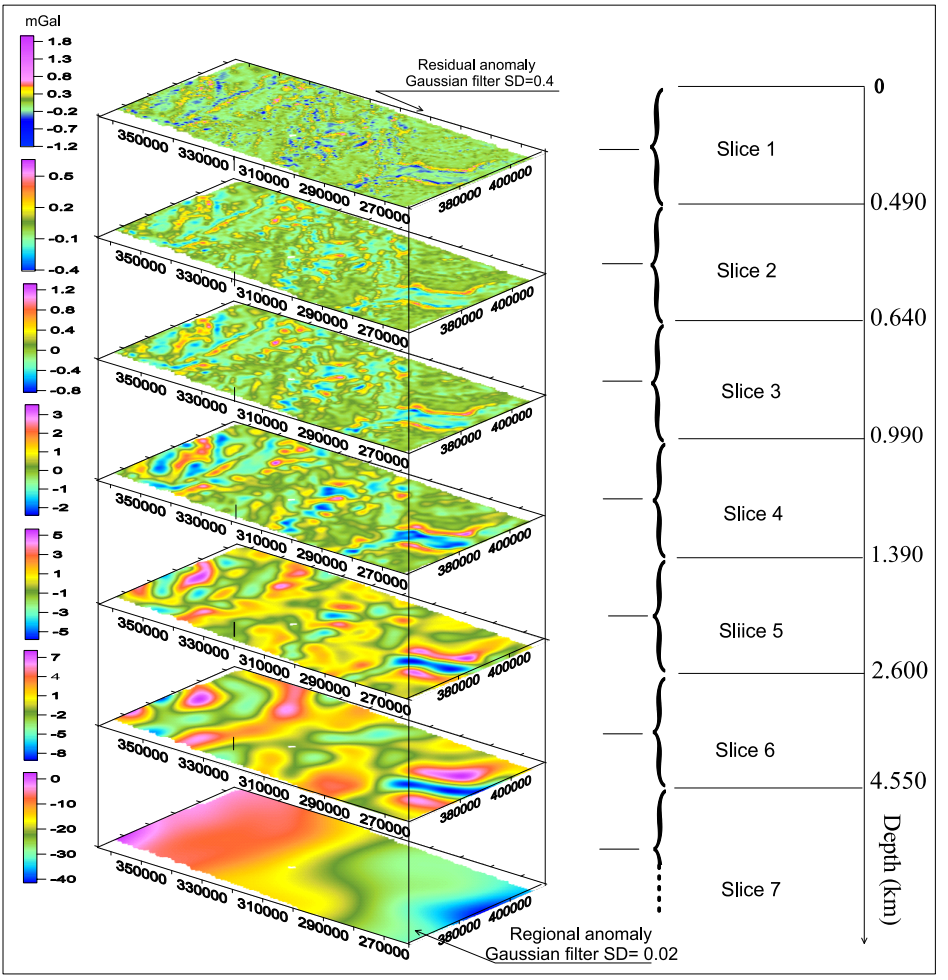

Fig. 6. Successive decomposition of Bouguer anomaly, using the Gaussian filter.

equal to 0.02 cycle km^{-1}, shows a general linear trend extending from NNW to SSE. The northern zone is dominated by a general gravity high oriented east-west while the southern zone is characterized by a gravity low oriented NW–SE. Those zones are separated by a middle region characterized by an arch shaped high gradient following the NE–SW direction (Fig. 6). The analysis of the pseudo-depth sliced gravity shows an increase in the size of the anomalies and an attenuation of certain anomalies with depth.

The pseudo-depth slices 1, 2 and 3 correlate with the pseudo-depths of 0–490, 490–640, and 640–990 m, respectively. Their gravity effects show dominate anomaly directions: E–W in the north, NW–SE and NE–SW in the center and NW–SE in the south (Fig. 6). They show equally:

- An anomaly shape smoothing with depth; thus, the positive anomaly of Sidi Dkril located in the East of Jebel Hairech and between Oued Mejarda and Oued Mellègue, is composed of two anomalies on the pseudo-depth slices 1 and 2, which merge into one in the pseudo-depth slice 3. This expresses the gravity effect of a near surface fault affecting the source of this anomaly but the lack of its persistence with depth suggests it is not a major fault.
- Good correspondence between gravity anomalies and outcropping series despite the exception of the uncorrelated anomalies observed in the Mio-Pliocene and quaternary deposits. This correspondence shows a general continuity of those outcropping series in depth to a pseudo-depth of 1000 m.
- Negative anomalies are associated with the Triassic outcrops of Jebel Aiate (Oued Bou Adila), Jebel Debadib- Ben Gasseur and Mellegue dam sector while other Triassic outcrops in the study area are associated with positive anomalies.
- Positive anomalies occur within Mio-Plio-Quaternary deposits of Mejarda basin. They extend for several kilometers along the E–W and NE–SW directions. They seem to be related to dense materials similar to Triassic, Jurassic and Cretaceous outcropping series, under thin Mio-Plio-Quaternary overburden. This suggests the Mejarda basin is more complex than a simple structural collapse basin. Notice in particular that positive anomalies attenuate significantly with pseudo-depth greater than 2 km (Slice 5 of Fig. 6).

The pseudo-depth slices 4, 5 and 6 correspond to the pseudo-depth ranges: 990 to 1390, 1390 to 2600 and 2600 to 4550 m, respectively. The gravity maps associated with these slices are characterized by NW–SE and NE–SW anomalies which become more dominant at greater depths (Fig. 6). The pseudo-depth slices 4, 5 and 6 show:

- All anomalies associated with outcrop structures are totally attenuated from the slice 5 or a pseudo-depth equal to 2600 m. Thus, the negative

anomalies on the Triassic outcrops of Jebel Aiate (Oued Bou Adila) and Mellegue dam sector disappear at the pseudo slice 4, indicating a vertical continuity of Triassic outcrop materials to a pseudo-depth equal to 1400 m. The negative anomaly associated with salt Triassic outcrops of Jebel Ben Debadib- Gasseur disappears completely at the pseudo-depth slice 5. This suggests that these outcrops are rooted to a pseudo-depth of 2600 m.

- A progressive attenuation with depth of NW–SE negative anomalies associated to El Marja, Oued Er Rmel and Zouarin basins. By pseudo-depth slice 5 they are reduced to one single anomaly. A similar effect is observed in the El Kef Plain, where the succession of positive and negative anomalies associated with high and collapsed zones continue to pseudo-depth slice 4; this succession is represent by a negative anomaly in the gravity map of slice 5.
- Positive anomalies associated with dense structures under Mio-Plio-Quaternary deposits attenuate with depth until they disappear entirely.
- The NW–SE anomalies of the middle domain are continuous with depth. For pseudo- depth slices 1 through 4, the NE–SW trends have more continuity and they truncate the NW–SE trends. But for depth slices 5 and 6, the NW–SE trend truncate the NE–SW anomalies.

3.4. Multiscale discontinuities and boundary identification

Next, the total horizontal gradient filter is applied to the gravity anomalies of pseudo-depth slices resulting from the successive decomposition of Bouguer anomaly. This permits identification of abrupt density variation zones with depth (Fig. 7). The total horizontal gradient of the gravity anomaly of deeper slice (7) (regional anomaly determiner with the Gaussian filter of standard deviation equal to 0.02 cycle km^{-1}) shows discontinuities of density for depths greater than 4550 m. It shows an important NW–SE discontinuity which corresponds with the deep fault identified by *Arfaoui et al. (2015)*. This fault cuts a NE–SW fault to the east of El Kef. These are the dominant structural directions at depth for this study area and show no correlation with the Triassic outcrops at the surface. But for the pseudo-depth slice 6 (2600 m) some of the surface faults begin to become apparent.

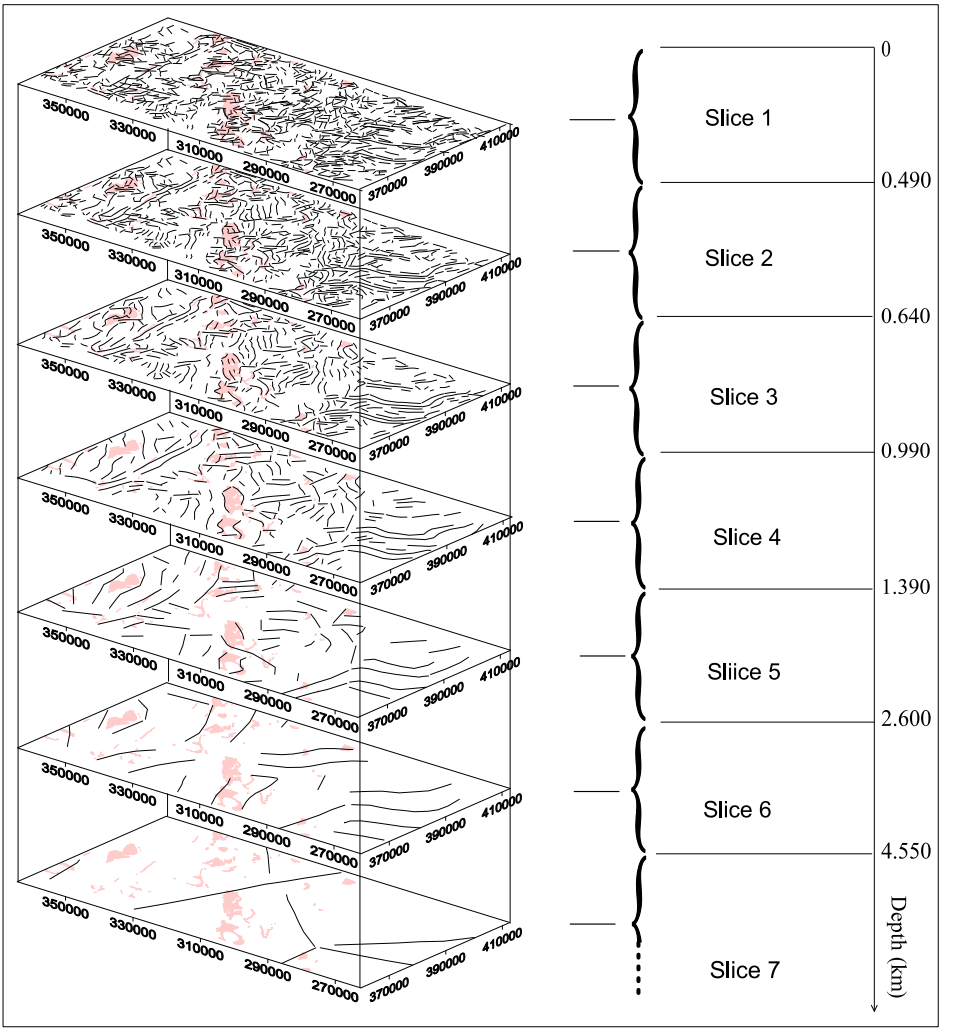

Fig. 7. Multiscale discontinuities and boundaries derived from the total horizontal gradient. Triassic outcrops is indicate in red color.

For example, the border faults of El Kalaa Khasba trough, the north fault oriented E–W that ties this trough to the Ouled Boughanem trough, the two faults limiting the Jebel Hairech structure, and the faults constituting the southern limit of the Mejarda basin all show some expression (Fig. 7). Both areas of the high total horizontal gradient surround the Ben Gasseur

Triassic structure; they indicate zones of abrupt density variations at this depth. Besides, they provide the Triassic series disturbance in this area. At this pseudo-depth the NW–SE fault is interrupted at El Kef apparently as a result of the Triassic materials rising. The NW–SE and NE–SW structural directions are still dominant over the middle domain structures (Fig. 7).

The pseudo-depth slice 5 (1400 m) shows:

- The south fault between the Ouled Boughanem and El Kalaa Khasba troughs. This south fault is relatively shallower than the northern fault, whose direction is close to E–W.
- N–S faults affecting the NW–SE and NE–SW fault of the southern border of Mejarda basin and the E–W faults that begin to appear in this basin.
- The NE–SW faults affect NW–SE faults in the middle domain. This is more indication of the change in the direction of the dominant faults mentioned previously.
- The strike-slip faults limiting the structures of Jebel Hairech, Kef El Jebel Agab and Chouichia, which evolved particularly to the SE.
- The discontinuities bordering the Ben Guasseur Triassic structure extend northwards towards Jebel Debadib. Extension of this area to the east is highly probable including the Zag Et Tir sector. Similarly, the bounding faults of the Sidi Dkril positive gravity anomaly in SE of Jebel Hairech appear to extend to this depth.

At the pseudo-depth slice 4 (1000 m), NE–SW faults dominate structures in the middle domain. They cut the NW–SE faults, especially on the emplacement of the deep NW–SE fault. The deepest NW–SE fault cuts a NE–SW fault at depth (slice 7), but at shallower depths (slice 4, 3.) the fault systems are changing. NE–SW discontinuities affect the NW–SE discontinuities suggesting a change of tectonic regime or a variation of its main direction.

At this pseudo-depth (1000 m), Triassic outcrops of Jebel Debadib including Ben Gasseur, the Mellègue Dam sector and Jebel Aiate (Oued Bou Adila) are clearly outlined by zones of maximum total horizontal gradient reflecting the vertical continuity of these structures. The two parallel E–W discontinuities in the Mejarda basin extend to the east for a greater distance. The bounding faults of the Jebel Hairech structure appear to be effected by other NE–SW faults. NW–SE faults begin to manifest in El Kalaa Khasba

trough (Fig. 7).

Moving to pseudo-depth slices 3 and 2 (less than 650 m), we see an increase in the number of discontinuities with a decrease of their lengths. With the exception of the bounding faults of El Kalaa El Khasba trough, all the faults discussed previously are cut by other faults. These include:

- The E–W Faults limiting Jebel Hairech that are affected by NE–SW and NW–SE faults.
- The E–W faults of Mejarda Basin.
- The faults bordering mini-basins of El Merja, Oued Er Rmel and Zouarine.
- The faults of E–W branch depression linking the El Kalaa El Khasba and Ouled Boughanem troughs.

Thus, the middle domain is characterized by two fault types differentiated by their directions: NE–SW and NW–SE. The NE–SW faults are the most dominant and they affect the NW–SE ones. Compared to the middle and southern domains, the northern domain is characterized by deep quiet structures that influenced by the activity of the EW and NE–SW faults at relatively superficial depth (Fig. 7). The multi-scale analysis using the total horizontal gradient of gravity slices allows for delineation of faults or geological contacts.

3.5. Apparent density pseudo-section derived from successive decomposition

The apparent density operator is applied generally, to generate density maps (*Gupta and Grant, 1985; Granser et al., 1989; Gupta and Sutcliffe, 1990; Keating, 1991; Singh et al., 2003; Arfaoui et al., 2011*). In our case we applied this operator to the gravity anomalies of pseudo-depth slices resulting from the successive decomposition of Bouguer anomaly, to generate density maps of pseudo-depth slices.

The process used to evaluate pseudo-sections describing density distribution at depth, consisted on the extraction of the apparent densities data of each profile from the apparent density maps and the attribution of a pseudo depth of the anomaly separation interface to these data. After, they are gridded by profile to generate apparent density pseudo-section.

Five isolated profiles of apparent density pseudo-sections are selected to examine important structural features (Fig. 8). The profiles adopted for this approach cross the mainly geologic structures of the study area: Mejarda Basin, salt structure of Jebel Debadib, El Marja-Oued Er Rmel and Zouarine basins and The Kalaa El Khaba through. The pseudo-sections PI and PII cross the positive and negative Bouguer anomalies of Mejarda basin. They show the presence of dense structures under the Mio-Plio-Quaternary overburden.

Indeed, the Sidi Dkril Bouguer anomaly is associated with a dense structure whose density varies between 2.38 and 2.48 g/cm^3. It is covered by deposits of 500 m thickness and a density ranging between 2.24 and 2.28 g/cm^3, (Fig. 9).

Two other high zones are located northwest of Oued Mliz and at Jebel Bou Rbah. They are covered by 500 m of Mio-Plio-Quaternary. However, the Oued Mliz and Oued Rarai areas and the southeastern part of Jebel Bou Rbah are characterized by thick Pliocene-Quaternary deposits with 2000 m of thickness (Fig. 10). The presence of Cretaceous and Eocene series at the base of collapsed zones is possible, especially since the density ranges between 2.34 to 2.36 g/cm^3. Directly below the high zones, the density decreases between 2000 and 4000 m depth (Fig. 10).

The pseudo-section density passing through Jebel Debadib shows a low density diapir shape with a rooting depth of 2000 m and a width of 4000 m (Fig. 11). At surface the density decreases from west to east (2.30 g/cm^3 to 2.23 g/cm^3), reflecting the heterogeneity of Triassic materials in this part of the diapir compared to the basal of the diaper portion that is homogeneous with a density less than 2.23 g/cm^3 (Fig. 11). The basal part of the diapir shows a Triassic series dip to the southeast which could explain the reduction of the rooting depth (1000 m) revealed previously in the Triassic outcrops of Jebel Aiate and Mellègue dam sector located further in the north.

The pseudo-density section of profile IV shows the structures of successive mini-basins of El Merja, Oued Rmel and Zouarine. It indicates an overburden of densities less than 2.28 g/cm^3 with thicknesses varying between 500 and 800 m. This overburden consisting of Mio-Pli-Quaternary deposits hides relatively dense terrains (2.32 g/cm^3) that are attributed to Eocene and Cretaceous rocks (Fig. 12).

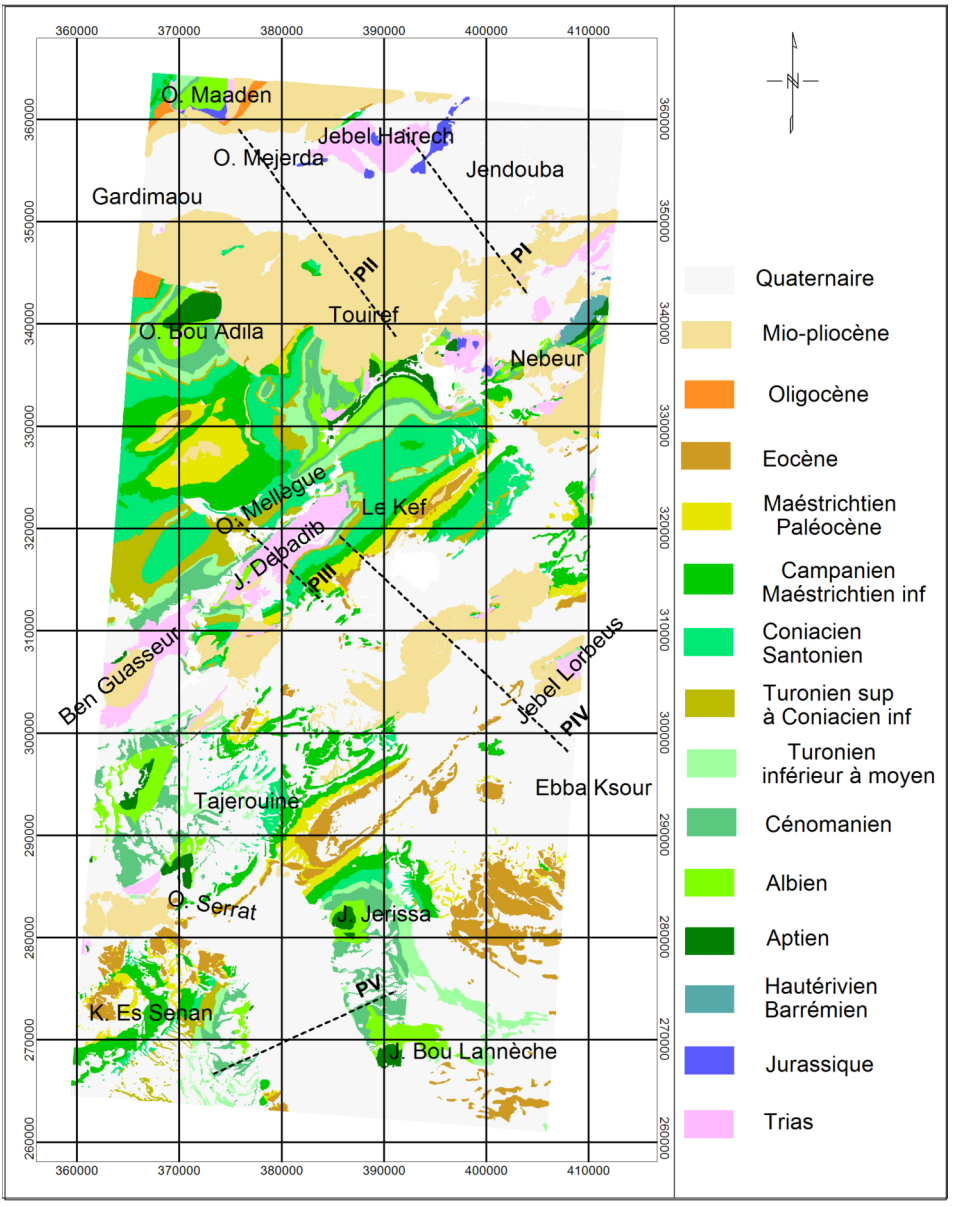

Fig. 8. Location of profiles used for the pseudo-section density imaging.

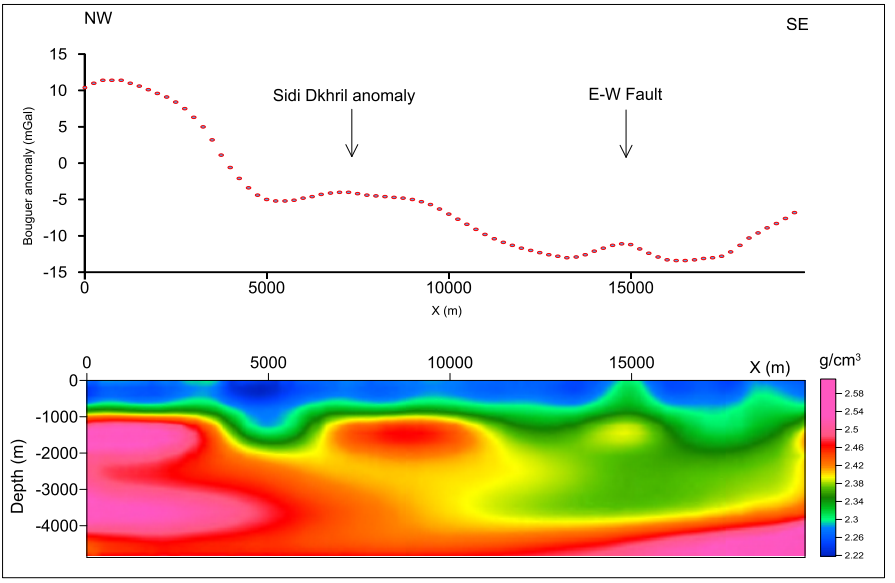

Fig. 9. Pseudo-section density of profile PI, Mejarda basin.

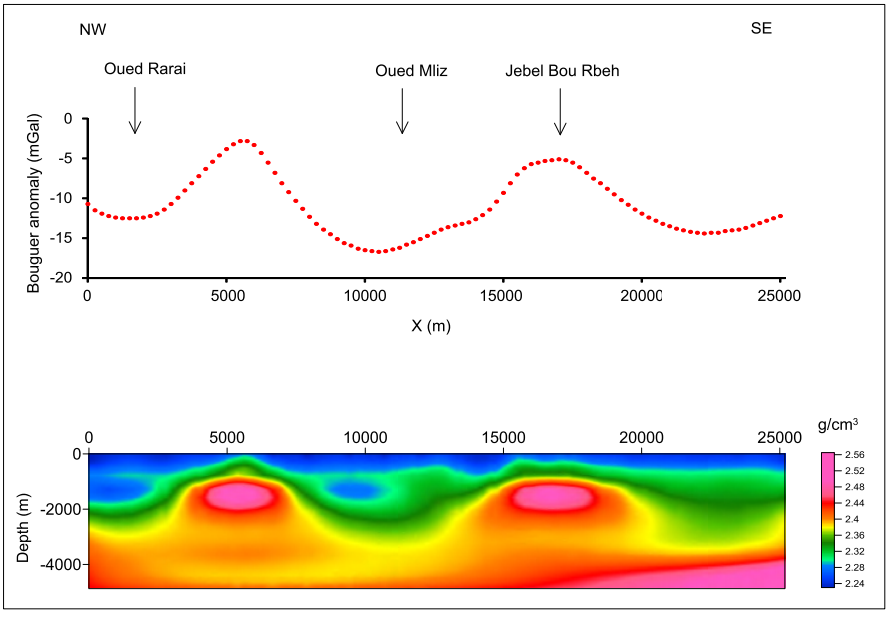

Fig. 10. Pseudo-section density of profile PII, Mejarda basin.

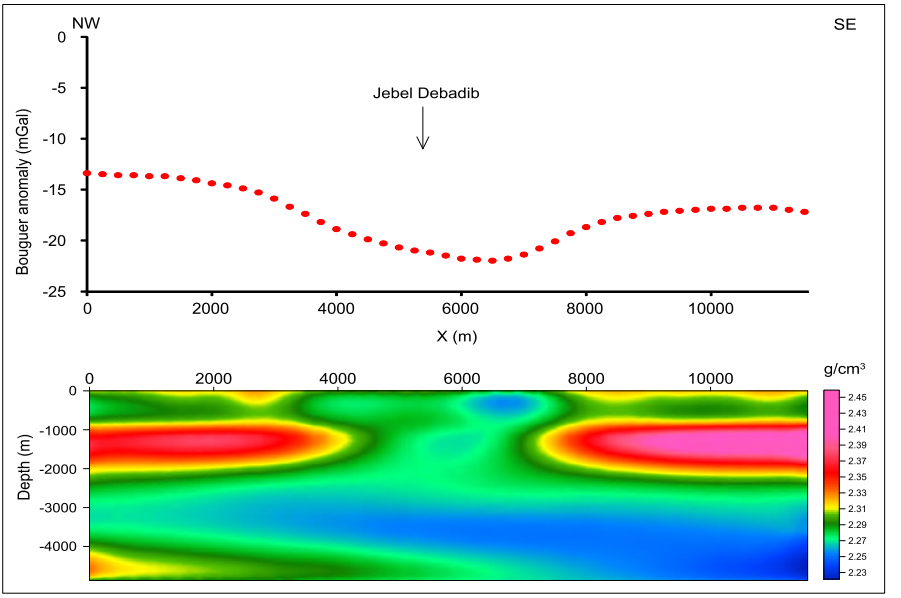

Fig. 11. Pseudo-section density of profile PIII, salt structure of Jebel Debadib.

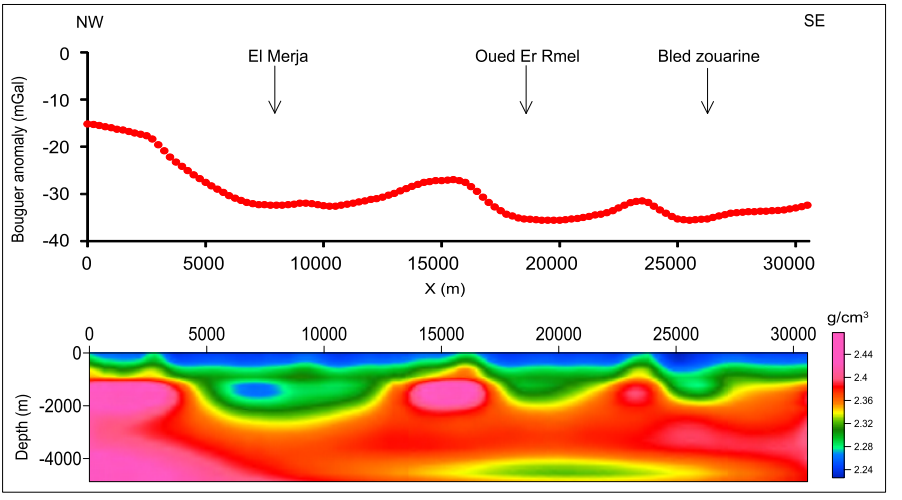

Fig. 12. Pseudo-section density of profile PIV, successive basins El Marja, Oued Er Rmel and Zouarine.

The distribution of the density in El Kalaa Khasba trough shows terrains of low density at the center (2.25 g/cm^3) traversed by relatively dense series (2.35 g/cm^3) at a depth of 1000 m (Fig. 13). This distribution could indicate the presence of Cretaceous and Triassic materials at depth. The density distribution also shows the bounding faults dip towards the center of the trough and that they are stopped at 2500 m depth. At this point two contacts appear to reverse toward the west and the east. These contacts combined with the density distribution beyond a depth of 2500 m, provide the appearance of a dome having two clearly distinguishable horizons defined by their densities. The deeper horizon sited at a depth greater than 4000 m has a density equal to 2.28 g/cm^3; it is surmounted by a dense horizon (2.34 g/cm^3), between the depths of 3500 m and 2500 m (Fig. 13). The dome seems to be Triassic, and agrees with the rise of Triassic materials started during the primary stages of formation of the Kalaa El Khasba trough (*Lehotsky and Bujnowsky, 1995*).

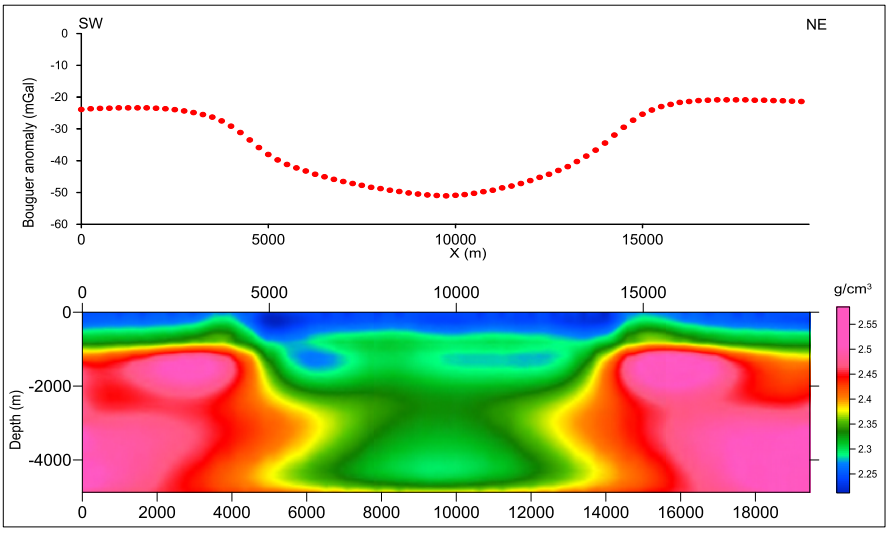

Fig. 13. Pseudo-section density of profile PV, Kalaa El Khasba.

4. Accuracy of the Results

The gravity of pseudo-slices available by the successive decomposition of Bouguer anomaly can be adopted to identify the discontinuities and geo-

logic contacts at different depths and to image density repartition on depth. These constitute a rapid interpretive approach improved by the total horizontal gradient and the apparent density operators. The results obtained correlate with the majority of surface geologic units and model the gravity structure effect as a density distribution following pseudo-section density. However, certain sources of error associated with this approach can cause discrepancies in results, as the depths of pseudo-slices and the background density used to calculate the apparent density maps. Depths of pseudo-slices are approximated by the spectral depth analysis method which corresponds to mean depths of the causative sources of anomalies in residual maps. However, the causative sources associated with the residual anomalies exist at different depths.

The densities used for transforming the gravity maps of pseudo-slices to apparent density maps are chosen from the values of measured density of surface rocks since we have no other control data. Background densities adopted are chosen as an increasing function with depth, but they remain a source of error which affects only the values of densities in the pseudo-depth sections. They do not affect the image of geologic structure in the pseudo-depth section resulting from the repartition of density since as the apparent density operator calculates a contrast of density independently of the background density, which is added at the end of the process as an average density.

Certainly, the resolution of the pseud-sections density and witch of multiscale discontinuities are affected by errors caused by the assessment process of depth and density. Taking into consideration the gravity survey scale (1/50000) and the spacing inter stations (1 km), we think that the results reflect regional model with an acceptable resolution accuracy ratio of the interpretative approach.

5. Conclusion

The multiscale interpretive approach based on the pseudo-depth slice gravity anomalies derived from the successive decomposition of Bouguer anomaly generally provided acceptable results compared to structural geological models in the study area. The use of depth spectral analysis makes this interpretive approach more capable of revealing the evolution of fault systems

and causative source boundaries with depth and equally to establish 2D pseudo-section density. The multiscale approach reveals deeper NW–SE and NE–SW faults compared to the relatively superficial N–S and E–W faults. It indicate that the excess of mass anomaly presented by the basins of the study correspond to Triassic, Cretaceous and/or Eocene dense rocks sited at relatively shallow depth under the Mio-Pliocene and Quaternary deposits. The salt Triassic outcrops of Jebel Debadib provide a diapir model with a homogeneous basal layer dipped to southeast. The basement under the Kalaa El Khasba trough is a Triassic dome.

Acknowledgements. We would like to express our thanks to the Office National des Mines (Tunisia) for permission to use the gravity data of the study region. Many thanks also to the technical editor and reviewer for their constrictive suggestions that improved the final version of this manuscript substantially.

References

Amiri A., 2013: Apport de la géophysique appliquée à la modélisation géodynamique de la moyenne valée de Mejarda. PhD. Thesis., Université Tunis El Manar, Faculté des sciences de Tunis (in French).

Arfaoui M., Inoubli M. H., Tlig S., Alouani R., 2011: Gravity analysis of salt structures. An example from the El Kef-Ouargha region (northern Tunisia). Geophysical Prospecting, **59**, 576–591.

Arfaoui M., Inoubli M. H., 2013: Advantages of using the kriging interpolator to estimate the gravity surface, comparison and spatial variability of gravity data in the El Kef-Ouargha region (northern Tunisia). Arabian Journal Geosciences, **6**, 3139–3147.

Arfaoui M., Reid A., Inoubli M. H., 2015: Evidence for a new regional NW–SE fault and crustal structure in Tunisia derived from gravity data. Geophysical Prospecting, **63**, 1272–1283.

Bansal A. R., Dimri V., 2001: Depth estimation from the scaling power spectral density of nonstationary gravity profile. Pure and Applied Geophysics, **158**, 799–812.

Ben Haj Ali M., 1997: Carte géologique au 1/50000 de Jendouba. Feuille No 32. Office National des Mines. Tunisie.

Blakely R. J., Simpson R. W., 1986: Approximating edges of source bodies from magnetic or gravity anomalies. Geophysics, **51**, 1494–1498.

Burollet P. F., 1991: Structures and tectonics of Tunisia. Tectonophysics, **195**, 359–369.

Burollet P. F., Sainfeld P., 1956a: Carte géologique au 1/50 000 d'El Kef. Direction des Mines et de la Géologie. Tunisie.

Burollet P. F., Sainfeld P., 1956b: Carte géologique au 1/50 000 de Tajerouine. Feuille No 50. Direction des Mines et de la Géologie. Tunisie.

Chihi L., 1995: Les fossés néogènes à quaternaires de la Tunisie de la mer pélagienne: leur signification dans le cadre géodynamique de la méditerranée centrale. PhD. Thesis., Université de Tunis El Manar (in French).

Chikhaoui M., 2002: La zone des diapirs en Tunisie: Cadre structural et évolution géodynamique de la sédimentation méso-cénozoïque et géométrie des corps triasiques. PhD. Thesis., Université de Tunis el Manar (in French).

Cooper G. R. J., Cowan D. R., 2006: Enhancing potential field data using filters based on the local phase. Computers & Geosciences, **32**, 1585–1591.

Cordell L., Grauch V. J. S., 1982: Mapping basement magnetization zones from aeromagnetic data in the San Juan Basin New Mexico. Presented at the Snd. Ann. Internat. Mtg. Sot. Explor. Geophys. Dallas, abstracts and biographies, 246–247.

Cordell L., Grauch V. J. S., 1985: Mapping basement magnetization zones from aeromagnetic data in the San Juan basin New Mexico. In Hinze W. J. Ed. The utility of regional gravity and magnetic anomaly maps Sot. Explor. Geophys, 181–197.

Fakhraoui M., Ghanmi M., Hatira N., 1998: Carte géologique au 1/50.000 De Nebeur. Feuille No 39. Office National des Mines. Tunisie.

Fedi M., Florio G., 2001: Detection of potential fields source boundaries by enhanced horizontal derivative method. Geophysical Prospecting, **49**, 40–58.

Ghanmi M., Vila J. M., Ben Youssef M., Jouirou M., Ben Kherouf F., 2000: Le matériel triasique interstratifié dans l'Albien de l'anticlinal autochtone atlasique du Jebel Takrona (Tunisie): Stratigraphie Arguments gravimétriques signification dans la transversale N–S des confins algéro-tunisiens (Maghreb du Nord-Est). Bulletin Sciences Histoires Naturelles, **136**, 19–27 (in French).

Gupta V. K., Ramani N., 1980: Some aspects of regional-residual separation of gravity anomalies in a Precambrian terrain. Geophysics, **45**, 1412–1426.

Gottis C., Sainfeld P., 1955: Carte géologique au 1/50.000 de Ghardimaou. Feuille No 31. Direction des Mines et de la Géologie. Tunisie.

Gupta V. K., Grant F. S., 1985: Mineral exploration aspects of gravity and aeromagnetic surveys in the Sudbury-Cobalt area, Ontario. SEG; The Utility of Regional Gravity and Magnetic Anomaly Maps, W. J. Hinze (Editor), 392–411.

Gupta V. K., Sutcliffe R. H., 1990: Mafic-ultramafic intrusives and their gravity field: Lac des Iles area, northern Ontario. Geological Society of America Bulletin, **102**, 1471–1483.

Granser H., Meurers B., Steinhauser P., 1989: Apparent density mapping et 3D gravity inversion in the eastern Alps. Geophysical Prospecting, **37**, 225–330.

Keating P., 1991: Density mapping from gravity data using Walsh transform. Geophysics, **57**, 637–642.

Keating P., Pilkington M., 2004: Euler deconvolution of the analytic signal and its application to magnetic interpretation. Geophysical Prospecting, **52**, 165–182.

Last B. J., Kubik K., 1983: Compact gravity inversion. Geophysics, **48**, 713–721.

Lehotsky I., 1979: Carte géologique au 1/50.000 d'Ebba Ksour. Feuille No 52. Office National des Mines. Tunisie.

Lehotsky I., Bujnowsky A., 1995: Carte géologique au 1/50.000 de Kalaat Es Senan. Feuille No 59. Office National des Mines. Tunisie.

Mahjoub K., 1997: Carte géologique au 1/50.000 de Les Salines. Feuille No 45. Office National des Mines. Tunisie.

Mahjoubi H., 1978: Un exemple de gisement ferrifère en un milieu recifal, Jerissa (Tunisie). PhD. Thesis., Univesité de Tunis.

Mareschal J. C., 1985: Inversion of potential field data in Fourier transform domain. Geophysics, **50**, 685–691.

Maus S., Dimri V., 1996: Depth estimation from the scaling power spectrum of potential fields? Geophysical Journal International, **124**, 113–120.

Miller H. G., Singh V., 1994: Potential field tilt – A new concept for location of potential field sources. Journal of Applied Geophysics, **32**, 213–217.

Murthy I. V. R., Rao P. R., 1993: Inversion of gravity and magnetic anomalies of two-dimensional polygonal cross sections. Computer Geosciences, **19**, 1213–1228.

Muzaffer O. A., Ünal D., 2013: Edge detection of magnetic sources using enhanced total horizontal derivative of the tilt angle. Bulletin of the Earth Sciences Application and Research, Centre of Hacettepe University.

Negi J. G., Dimri V. P., Agrawal P. K., Petey O. P., 1986: A spectral analysis of the profiles for thickness estimation of flood basalt of India. Exploration Geophysics, **17**, 105–111.

Nettleton L. L., 1942: Gravity and magnetic calculation. Geophysics, **7**, 293–310.

Ould Begga M. A., 2003: Evolution tectono-sédimentaire et analyse structural d'un segment des magrébides orientales: la région de Ghardimaou-Fernana (Tunisie Nord occidentale). PhD. Thesis., Université El Manar, Faculté des sciences de Tunis (in French).

Pawlowsky R. S., Hansen R. O., 1990: Gravity anomaly separation by Wiener filtering. Geophysics, **55**, 539–548.

Perthuisot V., 1978: Dynamique et pétrogenèse des extrusions triasiques en Tunisie septentrionale. PhD. Thesis., Ecole Normale Supérieure Paris (in French).

Perthuisot V., Aoudjehane M., Bouzenoune A., Hatira N., Laatar E., Mansouri A., 1998: Les corps triasiques des monts du Mellègue (confins algéro – tunisiens) sont-ils des diapirs ou des "glaciers de sel". Bulletin de la Société géologique de France, **169**, 53–61 (in French).

Reid A. B., Allsop J. M., Granser H., Millett, A. J., Somerton I. W., 1990: Magnetic interpretation in three dimensions using Euler deconvolution. Geophysics, **55**, 80–91.

Rouvier H., Henry B., Le Goff M., Hatira N., Laatar E., Mansouri A., 1998: Preuves paléomagnétiques de la non-interstratification des évaporites du Trias dans l'Albien du Maghreb oriental. Comptes Rendus de l'Académie des Sciences, **326**, 363–368 (in French).

Sainfeld P., 1951 : Carte géologique au 1/50000 d'Ouargha. Feuille No 38. Direction des travaux publics. Tunisie.

Salem A., Ravat D., 2003: A combined analytic signal and Euler method (AN-EUL) for automatic interpretation of magnetic data. Geophysics, **68**, 1952–1961.

Simpson S. M., 1954: Least- squares polynomial fitting to gravitational data and density plotting by digital computer. Geophysics, **19**, 808–811.

Singh A. P., Michra D. C., Axman G., 2003: Apparent density mapping and 3D gravity inversion of Dharwar crustal province. Journal of Indian Geophysical Union, **7**, 1–9.

Smati A., 1986: Les Gisements de Pb-Ba et de Fe du Jebel Slata (Tunisie du centre-nord) : minéralisations épigénétiques dans le crétacé néritique de la bordure d'un diapir de Trias, gisements de Sidi Amor Ben Salem et de Slata-Fer. PhD. Thesis., Université Pierre et Marie Curie Paris VI (in French).

Spector A., Grant F. S., 1970: Statistical models for interpreting aeromagnetic data. Geophysics, **35**, 293–302.

Talwani M., Worzel J. L., Letisman M., 1959: Rapid gravity computations for twodimensional bodies with application to the Mendocino submarine fracture zone. Journal of Geophysical Research, **64**, 49–59.

Talwani M., Ewing M., 1960: Rapid computation of gravitational attraction of threedimensional bodies of arbitrary shape. Geophysics, **25**, 203–225.

Thompson D. T., 1982: EULDPH: A new technique for making computer assisted depth estimates from magnetic data. Geophysics, **47**, 31–37.

Thurston J. B., Smith R. S., 1997: Automatic conversion of magnetic data to depth, dip, susceptibility contrast using the SPI^{TM} method. Geophysics, **62**, 807–813.

Verduzco B., Fairhead J. D., Green C. M., Mackenzie C., 2004: New insights into magnetic derivatives for structural mapping. The Leading Edge, **23**, 116–119.

Vila J. M., Ben Youssef M., Charriere A., Chikhaoui M., Ghanmi M., Kamoun F., 1994: Découverte en Tunisie, au SW du Kef, de matériel salifère triasique interstratifié dans l'Albien: Extension du domaine à "glacier de sel" sous-marin des confins algéro-tunisiens. Comptes Rendus de l'Académie des Sciences, **318**, 1661–1667 (in French).

Vila J. M., Ben Youssef M., Chikhaoui M., Ghanmi M., 1996: Un grand "glacier de sel" sous marin albien moyen du Nord-Ouest tunisien (250 Km^2?): Le matériel salifère triasique du "diapir" de Ben Gasseur et de l'anticlinal d'El Kef. Comptes Rendus de l'Académie des Sciences, **322**, 221–227 (in French).

Werner S., 1953: Interpretation of Magnetic Anomalies at Sheet-like Bodies. Sveriges Geologiska Undersokning, Arsbok, **43**, 6.

Wijns C., Perez C., Kowalczyk P., 2005: Theta map: Edge detection in magnetic data. Geophysics, **70**, 39–43.

Zaier A., 1999a: Carte géologique au 1/50000 d'Ain Ksiba. Feuille No 60. Office National des Mines. Tunisie.

Zaier A., 1999b: Evolution tectono-sédimentaire du basin phosphate du centre-ouest de la Tunisie Minéralogie, pétrographie, géochimie et genèse des phosphorites. PhD. Thesis., Université de Tunis II, Faculté des sciences de Tunis (in French).